Available online at www.sciencedirect.com
ScienceDirect
Journal of Power Sources 159 (2006) 1105–1114
JOURNAL OF POWER SOURCES
www.elsevier.com/locate/jpowsour

Semi-empirical model to elucidate the effect of methanol crossover on direct methanol fuel cell

Hung-Chi Tu [a], Yung-Yun Wang [a], Chi-Chao Wan [a,*], Kan-Lin Hsueh [b]

[a] *Department of Chemical Engineering, National Tsing-Hua University, Hsinchu 300, Taiwan*
[b] *Materials Research Laboratories of Industrial Technology Research Institute, Chutong, Hsinchu 310, Taiwan*

Received 4 November 2005; received in revised form 16 December 2005; accepted 20 December 2005
Available online 15 February 2006

Abstract

A semi-empirical equation was proposed to simulate the behavior of a direct methanol fuel cell (DMFC). The individual voltage losses in a DMFC due to methanol crossover and the overpotentials of both the cathode and anode can be distinguished. Three sets of experiments were designed and carried out to account for the three voltage losses. The values of each parameter in the model were then calculated and the computation showed that the fitted result and the experimental data were well matched. The relation between each significant phenomena and each parameter is discussed. The model quantitatively identified the major voltage losses to be both the sluggish reaction of methanol oxidation on the anode and the slow oxygen reduction on the cathode. The impact on cell performance by manipulating individual parameters is also discussed.

Keywords: Direct methanol fuel cell; Model; Methanol crossover

1. Introduction

The DMFC is a good potential portable power source due to its low operating temperature (room −60 °C) and high theoretical energy density (∼5000 Wh L^{-1}). At present, a low power density and a high catalyst loading of the membrane electrode assembly (MEA) are the major barriers that inhibit its commercialization. To improve the MEA power density, we need to analyze the MEA behavior and identify the critical factors that limit power density. However, the behavior inside the MEA is extremely complicated and heavily dependent on the operating condition, the constituting materials, the MEA structure, and the manufacturing procedure, etc. [1–6]. Thus, theoretical models or semi-empirical equations have been developed in order to predict and analyze factors which affect the performance.

The power curve of proton exchange membrane fuel cells (PEMFC) have been extensively studied. In general, they can be divided into three regions, the active, the ohmic and the mass-transfer limiting regions [7–10]. In the low current density region, the activation overpotential of oxygen reduction at the cathode predominates. In the intermediate region, the cell internal resistance, mainly contributed by the membrane resistance, becomes the major factor resulting in a linearly decreasing section of the discharge curve. In the high current density region, the overall cell reaction rate is limited by the depletion of reactants. Consequently, the mass-transfer overpotential becomes the dominant factor and it induces a sharp decay in the power density.

Many semi-empirical models have been proposed to describe the fuel cell power curve [2,3,7–10]. These models serve to distinguish the potential drop terms individually. Table 1 summarizes several important semi-empirical equations for the PEMFC. In 1988, Srinivasan et al. [7] presented a semi-empirical equation to describe the discharge behavior of a PEMFC. This equation contains a logarithmic term for the activation overpotential and a linear term for the ohmic drop. This equation is based on the Tafel equation and can perfectly describe the polarization curve before reaching the mass-transfer limiting region. Kim et al. [8] then added an exponential term to account for the mass-transfer overpotential. Although Kim's equation can fit the whole curve well, this exponential term is merely data fitting and has no physical meaning. So it was revised by Squadrito et al [9] and Chu and Jiang [10] with some theoretical reasoning.

* Corresponding author. Tel.: +886 3 5715131 3660; fax: +886 3 5715408.
E-mail address: ccwan@mx.nthu.edu.tw (C.-C. Wan).

0378-7753/$ – see front matter © 2006 Elsevier B.V. All rights reserved.
doi:10.1016/j.jpowsour.2005.12.052

Nomenclature

Symbols

A_{cat}	Actual available catalyst area
A_{MEA}	The MEA cross-section area
B	Tafel slope
$C_{in,ch}$	The methanol concentration on the anodic GDL surface
$C_{in,cat}$	The methanol concentration at the interface between GDL and the catalyst layer
C^{ref}	The reference methanol concentration
E	Electrode potential
E_{cell}	Cell voltage
E_{cross}	The intrinsic voltage loss due to methanol crossover
$E_{r,ME}$	The reversible electrode potential of methanol oxidation
E_{r,O_2}	The reversible potential of oxygen
E_0	Defined in Eq. (7) for anodic part and Eq. (13) for cathodic part
F	Faradaic constant
I	Current
i^*	The apparent current density
i_o^*	The apparent exchange current density at the reference concentration of methanol or partial pressure of the oxygen
$i^*_{cross,OCP}$	The apparent current density resulting from crossover at the open circuit potential
$k_{cl,ME}$	The methanol mass-transfer coefficients inside GDL
k_{eff}	The effective mass-transfer coefficient inside the GDL
m	Equal to the reaction order multiplied by the Tafel slope
N	The mass flux of methanol
n	The inverse of the apparent limiting current density
$P_{in,ch}$	The oxygen partial pressure at the GDL surface
$P_{in,cat}$	The partial pressure at the interface between GDL and cathodic catalyst layer
P^{ref}	The reference partial pressure of oxygen
R_{cell}	The internal cell resistance
r	The reaction order
z	The equivalent of specie

Greek symbols

α	The charge-transfer coefficient
δ	The proportional constant
θ	An empirical factor which represents the ratio of the oxygen reversible potentials with and without methanol existing

Suffix

a	Anode
c	Cathode

Table 1
The empirical equations for a PEMFC

Equation	References
$E = E_0 - b\log i - Ri$	Srinivasan et al. [7]
$E = E_0 - b\log i - Ri - m\exp(ni)$	Kim et al. [8]
$E = E_0 - b\log i - Ri - \alpha i^k \ln(1-\beta i)$	Squadrito et al. [9]
$E = E_0 - b\log i - Ri - i_m m\exp(ni_m)$	Chu and Jiang [10]

The same approach has been applied to the DMFC. Scott et al. [11] proposed a simplified equation in which the anodic mass-transfer overpotential was represented by the concentration overpotential of methanol. Scott and coworkers [12] found that Kim's equation was unsatisfactory in the low concentration case. In contrast, Squadrito's equation did show perfect fittings under all testing conditions but it needed heavy computing to solve the equations. Thus, Scott's group presented a modified equation as follows:

$$E_{cell} = E_0^* - b\log i - R_e i + C_1 \ln(1 - C_2 i) \quad (1)$$

In 2003, Scott and coworkers [13] based on the Tafel approximation developed a formula similar to Eq. (1), in which each parameter (E_0^*, b, R_e, C_1 and C_2) has its physical meaning. Evaluation of individual parameters could help identify the key factor that causes decay of cell performance.

However, most semi-empirical equations could not separate the anodic voltage loss from the cathodic voltage loss. This is acceptable for the PEMFC because the anodic overpotential is minor and can be ignored. Unlike the PEMFC, methanol crossover from anode to cathode and the sluggish reaction of methanol oxidation on the anode are two unique characteristics of a DMFC. The methanol crossover is due to the diffusion and the osmostic drag of methanol from anode to cathode. It not only lowers the output voltage of a DMFC but also reduces the utilization efficiency of methanol fuel. The sluggish oxidation of methanol causes an additional activation overpotential loss at the anode. Consequently, the equations listed in Table 1 are not adequate for a DMFC.

Thus, we have developed a semi-empirical model for a DMFC by taking these two important factors into account. Moreover, this model could separate the anodic and the cathodic performances individually with a clear crossover effect. Major voltage losses of the DMFC can then be identified from its power delivery curve.

2. Theoretical derivation

Fig. 1(a) is a basic sketch of the MEA structure of a DMFC including flow fields, gas diffusion layers (GDLs), catalyst layers on both electrodes and the membrane. The GDL is made of carbon paper or carbon cloths that have large pores for fast diffusion of species. The catalyst layers have a fine pore structure and a large surface area so that the species react with a minimum amount of catalyst. At the anode–membrane interface, the residue methanol will cross to the cathode due to osmostic drag and diffusion. Fig. 1(b) depicts the methanol concentration distribution on the anodic side and the oxygen pressure on the

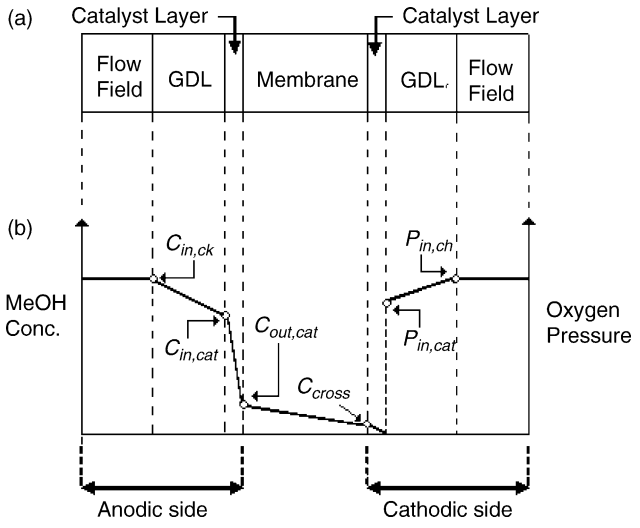

Fig. 1. (a) A simplified structure of the DMFC MEA; (b) the methanol concentration and oxygen pressure profile at different positions.

cathodic side. At steady state, two assumptions were made inside the GDL: (i) only the mass transport of species occur and (ii) the reactant flux is proportional to the concentration gradient.

Inside the anodic GDL, the mass flux of methanol (N_{ME}) is directly proportional to the difference of methanol concentration on the GDL surface ($C_{in,ch}$) and at the interface between GDL and the catalyst layer ($C_{in,cat}$).

$$N_{ME} = k_{cl,ME}(C_{in,ch} - C_{in,cat}) \tag{2}$$

where $k_{cl,ME}$ is the methanol mass-transfer coefficients inside GDL.

If methanol crossover flux does not exist, all methanol which diffuses from the GDL should be electrochemically oxidized to carbon dioxide on the anodic catalyst layer. However, a DMFC has significant methanol crossover from the anode to the cathode [2–4,14–17]. The amount of methanol crossover could be treated as linearly decreasing with increasing current density [18–21]. The material balance of methanol on the anode can be described by Eq. (3). The amount of methanol diffusing from the GDL to the anodic catalyst layer ($N_{ME}A_{MEA}$) is equal to the sum of (i) methanol consumed in the catalyst layer (I_a in Eq. (3)) and (ii) the amount of methanol diffusing and migrating to cathode ($I_{cross,OCP} - \delta I_a$).

$$N_{ME}A_{MEA} = \frac{I_a + (I_{cross,OCP} - \delta I_a)}{z_a F} \tag{3}$$

where $I_{cross,OCP}$ is the equivalent current due to crossover at the open circuit potential, δ a ratio describing how the crossover flux decreases with increasing current, z_a the chemical equivalent of methanol, F Faradic constant, and A_{MEA} the cross-section area of MEA, respectively.

The anodic current density should be equal to the anodic current (I_a) divided by the actual catalyst area ($A_{cat,a}$). However, the total active area is difficult to measure and it changes with various manufacturing methods. Therefore, the MEA cross-section area (A_{MEA}) was used in our analysis instead of $A_{cat,a}$. Accordingly, the current densities in Eq. (4) become the apparent current densities (i_a^* and $i_{cross,OCP}^*$), which are equal to the current divided by A_{MEA}.

$$N_{ME} = \frac{i_a^* + (i_{cross,OCP}^* - \delta i_a^*)}{z_a F} \tag{4}$$

Substituting N_{ME} from Eq. (2) into (4), Eq. (5) was obtained.

$$(1-\delta)i_a^* + i_{cross,OCP}^* = k_{cl,ME} z_a F (C_{in,ch} - C_{in,cat}) \tag{5}$$

The apparent current density (i_a^*) and anodic potential (E_a) is assumed to follow the Tafel behavior as given by Eq. (6):

$$i_a^* = i_{oa}^* \left(\frac{C_{in,cat}}{C^{ref}}\right)^{r_a} \exp\left[\frac{\alpha_a z_a F}{RT}(E_a - E_{r,ME})\right] \tag{6}$$

where C^{ref} is the methanol concentration at a fixed reference condition, $E_{r,ME}$ the reversible electrode potential of methanol oxidation, r_a the reaction order of methanol, α_a the charge-transfer coefficient of methanol oxidation, and i_{oa}^*, the exchange current density of methanol oxidation at a reference methanol concentration, C^{ref}.

Eq. (5) coupled with Eq. (6) can be rearranged into Eq. (7), in which E_a is expressed as a function of i_a^*.

$$E_a = E_{0,a} + b_a \ln i_a^* - m_a \ln\{1 - n_a[(1-\delta)i_a^* + i_{cross,OCP}^*]\} \tag{7}$$

where

$$E_{0,a} = E_{r,ME} + b_a \ln \frac{1}{i_{oa}^*}\left(\frac{C^{ref}}{C_{in,ch}}\right)^{r_a}, \quad b_a = \frac{RT}{\alpha_a z_a F},$$

$$m_a = \frac{r_a RT}{\alpha_a z_a F}, \quad n_a = \frac{1}{z_a F k_{cl,ME} C_{in,ch}} = \frac{1}{i_{lim,a}^*}$$

The variable δ is defined to be the ratio of $i_{cross,OCP}^*$ to $i_{lim,a}^*$ (or $1/n_a$) as given by Eq. (8). The methanol crossover flux has the largest amount at the open circuit condition ($i_{cross,OCP}^*$), but it approaches 0 when i_a^* reaches the methanol mass-transfer limiting current density ($i_{lim,a}^*$) and $C_{in,cat}$ approaches 0.

$$\delta = n_a i_{cross,OCP}^* \tag{8}$$

When we combine Eq. (8) with Eq. (7), the anodic potential of DMFC can be expressed as follows:

$$E_a = E_{0,a} - E_{cross,a} + b_a \ln i_a^* - m_a \ln(1 - n_a i_a^*) \tag{9}$$

where

$$E_{cross,a} = m_a \ln(1-\delta)$$

The cathodic current density (i_c^*) can also be obtained similarly. The material balance of oxygen on the cathode can be described by Eq. (10) where $k_{eff,c}$ is the effective mass-transfer coefficient of oxygen inside the cathodic GDL and z_c is the chemical equivalent of oxygen. The right-hand-side of Eq. (10) represents the oxygen flux in GDL and is proportional to the difference of oxygen partial pressure at the GDL surface ($P_{in,ch}$) and the partial pressure at the interface between GDL and cathodic catalyst layer ($P_{in,cat}$). We visualized that the oxygen transported from GDL is reduced to i_c^* and consumed by the oxygen/methanol

redox reaction in the form of a local cell which should equal to $i^*_{\text{cross,OCP}} - \delta i^*_{\text{c}}$. So a material balance of oxygen leads to Eq. (10).

$$i^*_{\text{c}} + (i^*_{\text{cross,OCP}} - \delta i^*_{\text{c}}) = k_{\text{eff,c}} z_{\text{c}} F (P_{\text{in,ch}} - P_{\text{in,cat}}) \tag{10}$$

The oxygen reduction proceeds in parallel on the methanol-covered and fresh catalyst surfaces if methanol passes through the membrane [22]. On the methanol-free surface, oxygen reacts with the protons and electrons are released at the anode, as shown in Eq. (11).

$$i^*_{\text{c}} = i^*_{\text{oc}} \left(\frac{P_{\text{in,cat}}}{P^{\text{ref}}} \right)^{r_{\text{c}}} \exp \left[-\frac{\alpha_{\text{c}} z_{\text{c}} F}{RT} (E_{\text{c}} - E_{r,\text{O}_2}) \right] \tag{11}$$

where P^{ref} is the oxygen partial pressure at reference condition. $E_{\text{r,O}_2}$ is the reversible potential of oxygen. α_{c} and r_{c} are the charge-transfer coefficient and the reaction order of oxygen reduction, respectively, and i^*_{oc} is the apparent exchange current density of oxygen reduction at P^{ref}.

On the methanol-covered surface, the methanol oxidation and oxygen reduction form a redox couple. The amount of methanol crossover from the anode ($i^*_{\text{cross,OCP}} - \delta i^*_{\text{c}}$) is totally consumed at the cathode. Since the methanol is oxidized at much lower potential than the potential of oxygen reduction, whereby forming a local cell reaction. The presence of methanol accelerates the oxygen reduction and it should have a lower specific free energy on the methanol-covered catalyst surface [22]. On this surface, the methanol oxidation rate is equal to the oxygen reduction rate as given by Eq. (12).

$$i^*_{\text{cross,OCP}} - \delta i^*_{\text{c}} = -i^*_{\text{oc}} \left(\frac{P_{\text{in,cat}}}{P^{\text{ref}}} \right)^{r_{\text{c}}} \times \exp \left[-\frac{\alpha_{\text{c}} z_{\text{c}} F}{RT} (E_{\text{c}} - \theta E_{\text{r,O}_2}) \right] \tag{12}$$

where the empirical factor, θ, is always smaller than 1. Obviously, when θ equals unity, Eq. (12) returns to Eq. (11). It represents the diminution of free energy from a methanol-free surface to a methanol-covered surface.

Substituting i^*_{c} from Eq. (11) and $i^*_{\text{cross,OCP}} - \delta i^*_{\text{c}}$ from Eq. (12) into Eq. (10), Eq. (13) is obtained:

$$E_{\text{c}} = E_{0,\text{c}} + b_{\text{c}} \ln \left\{ 1 - \exp \left[-\frac{(1-\theta) E_{\text{r,O}_2}}{b_{\text{c}}} \right] \right\} - b_{\text{c}} \ln[(1-\delta) i^*_{\text{c}} + i^*_{\text{cross,OCP}}] + m_{\text{c}} \ln\{1 - n_{\text{c}}[(1-\delta) i^*_{\text{c}} + i^*_{\text{cross,OCP}}]\} \tag{13}$$

where

$$E_{0,\text{c}} = E_{\text{r,O}_2} - b_{\text{c}} \ln \frac{1}{i^*_{\text{oc}}} \left(\frac{P^{\text{ref}}}{P_{\text{in,ch}}} \right)^{r_{\text{c}}}, \quad b_{\text{c}} = \frac{RT}{\alpha_{\text{c}} z_{\text{c}} F},$$

$$m_{\text{c}} = \frac{r_{\text{c}} RT}{\alpha_{\text{c}} z_{\text{c}} F}, \quad n_{\text{c}} = \frac{1}{z_{\text{c}} F k_{\text{eff,c}} P_{\text{in,ch}}}$$

The apparent current density flowing out of the cathode (i^*_{c}) is equal to the apparent current density flowing out of the anode (i^*_{a}). To simplify the notation, we used the apparent current density i^* for i^*_{c} in Eq. (13) and for i^*_{a} in Eq. (9). The cell voltage (E_{cell}) is the difference between E_{c} and E_{a} if there is no internal resistance (R_{cell}). When R_{cell} is taken into account, the cell voltage E_{cell} is as follows:

$$\begin{aligned} E_{\text{cell}} &= E_{\text{c}} - E_{\text{a}} - R_{\text{cell}} i^* \\ &= (E_{0,\text{c}} + E_{\text{cross,c}}) - b_{\text{c}} \ln[(1-\delta) i^* + i^*_{\text{cross,OCP}}] \\ &\quad + m_{\text{c}} \ln\{1 - n_{\text{c}}[(1-\delta) i^* + i^*_{\text{cross,OCP}}]\} - E_{0,\text{a}} \\ &\quad + E_{\text{cross,a}} - b_{\text{a}} \ln(i^*) + m_{\text{a}} \ln(1 - n_{\text{a}} i^*) - R_{\text{cell}} i^* \end{aligned} \tag{14}$$

where we define a term $E_{\text{cross,c}}$, which equals $\ln\{1 - \exp[-(1-\theta) E_{\text{r,O}_2}/b_{\text{c}}]\}$, and its physical meaning will be explained later.

3. Experimental and numerical fitting procedure

The MEA used in our experiment had a carbon cloth as the GDL on both sides and its size was 10.89 cm^2 (3.3 cm × 3.3 cm). The anodic catalyst layer had 4 mg cm^{-2} PtRu black with a 1:1 atomic ratio. The cathodic catalyst layer contained 4 mg cm^{-2} Pt black. The proton exchange membrane was Nafion 117 from DuPont.

In order to calculate each parameter in Eq. (14), we did three sets of experiments. Experiment A (Exp A) was actually a PEMFC system fed with hydrogen at the anode. Since the anodic polarization can be neglected [7–10], Exp A can in fact give a measure of the cathodic performance of DMFC under the same condition. Experiment B (Exp B) provides regular DMFC discharging with methanol and air as feed. In Experiment C (Exp C), the cathode was fed with hydrogen so that cathodic polarization can be neglected [23] and the anodic performance of the DMFC can be identified. Table 2 listed the conditions used in each experiment. We chose flow rates higher than conventional figures in order to keep the input concentration constant and our assumption in the theoretical derivation that the reactant transfer is only dependent on diffusion and independent of the input flow rate is thereby justified.

Table 2
The flow rate and cell temperature settings in the experiments (10%, v/v ≈ 2.5 M)

Experiment	Anode		Cathode		Cell temp. (°C)
	Reactant	Flow rate (l min^{-1})	Reactant	Flow rate (l min^{-1})	
Exp A	H_2	1	Air	1	40, 60
Exp B	CH_3OH (10%, v/v)	0.15	Air	1	40, 60
Exp C	CH_3OH (10%, v/v)	0.15	H_2	1	40, 60

Table 3
The current scan rates and ranges for the different experiments

Experiment	Method			
	Low current		Large current	
	Scan rate (mA s^{-1})	Scan range (A)	Scan rate	Scan range (A)
Exp A	0.1	0–0.3	0.1 A min^{-1}	0.3–10
Exp B	0.1	0–0.3	0.025 A/30 s	0.3–3.5
Exp C	0.1	0–0.3	1 mA s^{-1}	0.3–0.7
AC impedance (at OCP)	To measure the cell resistance individually under open circuit potential after every test			

In these three experiments, the measuring instruments and conditions in the low current region were different from those in the high current density region. Table 3 lists the measuring conditions used in these two current ranges. In Exp A and Exp B, a potentiostat (Solartron 1280z) was employed to obtain the precise variation in the activation region at low currents (0–0.3 A) and the fuel cell test station (Electrochem. Fuelcell 2000) provided the polarization curve in the high current region (above 0.3 A). However, Exp C was totally done by the potentiostat because of the limitation of the test station. We also measured the cell resistance of each experiment at open circuit by AC impedance. The internal resistance of Exp B was used as the cell resistance (R_{cell}) in our analysis.

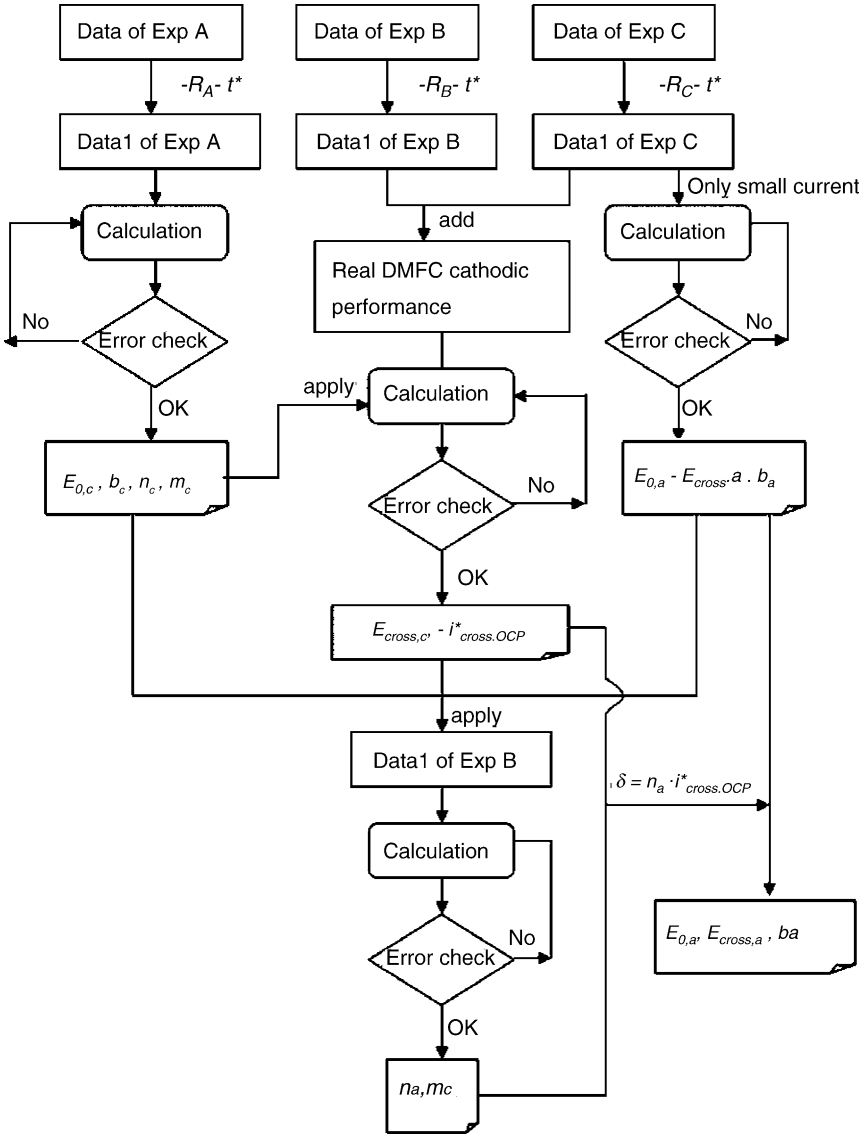

Fig. 2. The calculation procedure of the semi-empirical equation. R_A, R_B and R_C are the cell resistances of Exp A, Exp B and Exp C, respectively. Moreover, we also use R_B as R_{cell} in our semi-empirical model.

The parameters in Eq. (14) could be calculated by using least-square curve fitting. Cathodic parameters ($E_{0,c}$, b_c, $E_{cross,c}$, $i^*_{cross,OCP}$, m_c and n_c) and anodic parameters ($E_{0,a}$, b_a, $E_{cross,a}$, m_a and n_a) were calculated in a sequential manner from these three sets of data mentioned above. The calculation procedure is shown in Fig. 2. The internal resistance of Exp A (R_A), Exp B (R_B), and Exp C (R_C) were measured by the AC impedance technique. The ohmic overpotential resulting from the internal resistance was deducted before least-square curve fitting. Because the ohmic drop is beforehand eliminated, we only need to consider the activation overpotential and the concentration overpotential in our calculation. Accordingly, the effect of the concentration overpotential is enhanced in the polarization curve, so we can evaluate m and n even from data not totally in the limiting region.

Firstly, we calculated the cathodic parameters, $E_{0,c}$, b_c, m_c and n_c from data of Exp A. Due to the low current range of Exp C, ($E_{0,a} - E_{cross,a}$) and b_a could be obtained by neglecting the concentration overpotential or m_a and n_a. The sum of Exp B's and Exp C's polarization curves should be the actual cathodic performance of DMFC. In contrast, the polarization curve of Exp A should be the ideal cathodic performance because it has no crossover effect. Therefore, the cathodic parameter related to methanol crossover, $E_{cross,c}$ and $i^*_{cross,OCP}$, could be evaluated by fitting the deviation between ideal and actual cathodic polarization curve. Finally, the difference between the potential response calculated with the parameters already obtained and actual data of Exp B is represented by the $m_a \ln(1 - n_a i^*)$ term in Eq. (14). So m_a and n_a can be evaluated from this discrepancy. Moreover, $E_{0,a}$ and $E_{cross,a}$ are also separated easily according to the definition of $E_{cross,a}$ shown in Eq. (9).

4. Results and discussions

4.1. Model validations

The measured data of cell voltage versus current density (E_{cell} versus i^*) for different schemes are given in Figs. 3–5. The values of the parameters listed in Tables 4 and 5 were obtained by fitting Eq. (14) with the curves in the above figures except the resistances. The E_{cell} versus i^* curves calculated from these parameters are also plotted on the same diagram for comparison. This semi-empirical model obviously fits the experimental data very closely with H_2/air feeding, methanol/air feeding, or methanol/H_2 feeding at 40 and 60 °C. It should be noticed that

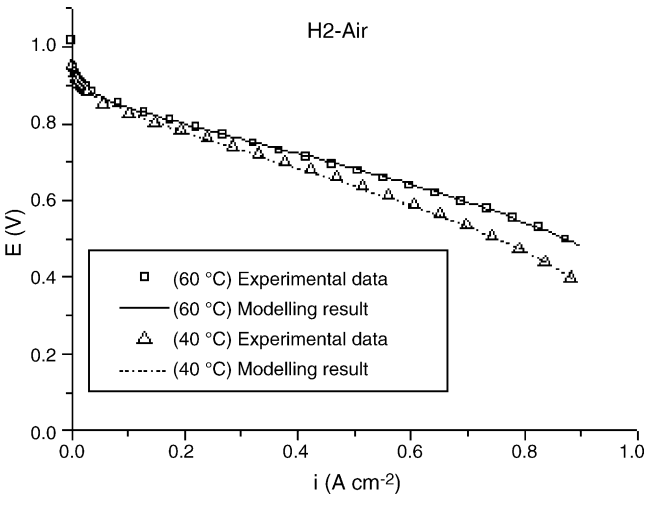

Fig. 3. The curve fitting result of Exp A.

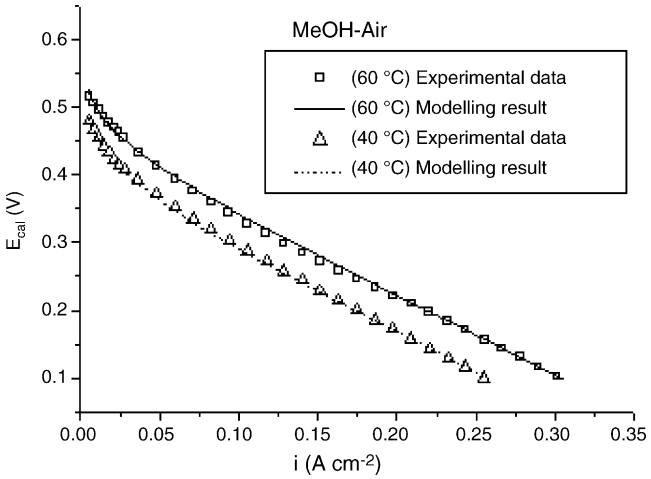

Fig. 4. The curve fitting result of Exp B.

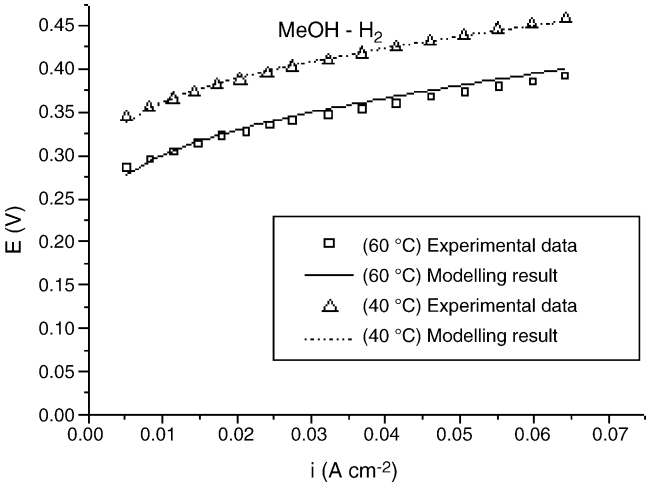

Fig. 5. The curve fitting result of Exp C.

Table 4
Parameters of semi-empirical model obtained by fitting the data at 40 °C

$E_{0,c}$ (V)	0.817
b_c (V e^{-1})	0.021
m_c (V e^{-1})	0.074
n_c (cm^2 A^{-1})	1.020
$E_{cross,c}$ (V)	−0.065
$i^*_{cross,OCP}$ (A cm^{-2})	0.030
$E_{0,a}$ (V)	0.493
b_a (V e^{-1})	0.031
m_a (V e^{-1})	0.051
n_a (cm^2 A^{-1})	2.660
$E_{cross,a}$ (V)	−0.004
R (Ω cm^2)	0.563

Table 5
Parameters of semi-empirical model obtained by fitting the data at 60 °C

$E_{0,c}$ (V)	0.827
b_c (V e^{-1})	0.021
m_c (V e^{-1})	0.056
n_c (cm^2 A^{-1})	0.997
$E_{cross,c}$ (V)	−0.064
$i^*_{cross,OCP}$ (A cm^{-2})	0.114
$E_{0,a}$ (V)	0.406
b_a (V e^{-1})	0.030
m_a (V e^{-1})	0.131
n_a (cm^2 A^{-1})	1.607
$E_{cross,a}$ (V)	−0.027
R (Ω cm^2)	0.579

the apparent resistance in Fig. 3 (slope in the linear region) was obtained with the membrane saturated with water (for hydrogen/air feeding). The resistances listed in Tables 4 and 5 were measured by the impedance method with the membrane saturated with a mixture of methanol and water (methanol/air feeding) due to methanol crossover. The resistance of the membrane saturated with water was lower than the resistance of the membrane saturated with methanol/water. This is reflected in the resistance difference between Fig. 3 and Tables 4 and 5. Several observations were made as follows:

(i) Because a higher temperature causes faster reaction kinetics of both methanol oxidation and oxygen reduction, the activation overpotential should decrease with increasing temperature. In other words, a lower $E_{0,a}$ and a higher $E_{0,c}$ are obtained when the temperature rises. Fitting results demonstrate the same trend as shown in Tables 4 and 5.

(ii) In the literature [4,16,22], b_a for methanol oxidation is in the range of 60–120 mV dec^{-1} (25.6–51.2 mV e^{-1}) and b_c for oxygen reduction should be around 60 mV dec^{-1} (25.6 mV e^{-1}). As shown in Tables 4 and 5, the value of b_a is in the predicted range, but the value of b_c is slightly lower. It is noteworthy that b_a and b_c are insensitive to the temperature variation within our experimental range. (The difference of b_a or b_c between 40 and 60 °C is only about 2 mV e^{-1}.) Therefore, the polarization is sensitive to temperature due to the changes of $E_{0,a}$ and $E_{cross,a}$ (or $E_{0,c}$ and $E_{cross,c}$ at the cathode) at different thermal settings. This will be discussed later.

(iii) m_a and m_c are related to mass transfer and are defined to be the reaction order multiplied by the Tafel slope. In the literature [18,19,24–26], the reaction orders of oxygen and methanol are usually equal to or less than unity. Therefore, m_a and m_c should be equal or less than b_a and b_c, respectively. However, the mass-transfer rates of methanol in the anode and oxygen in the cathode would be affected by other processes such as water flooding on the cathode, blocking of the methanol pathway by CO_2 bubbles on the anode. Therefore, m_a and m_c in Table 4 and Table 5 obtained by curve fitting of the experimental data were different from their theoretical value.

(iv) n_a and n_c should be equal to the reciprocals of the anodic and cathodic limiting current density and their values should decrease with increasing temperature. Our results in both Tables 4 and 5 are consistent with this prediction.

(v) Parameters related to methanol crossover ($i^*_{cross,OCP}$, $E_{cross,a}$, and $E_{cross,c}$) did not appear in any semi-empirical equation proposed in the literature before. $i^*_{cross,OCP}$ is the equivalent current density of the methanol crossover flux from the anode at open circuit. The value of $i^*_{cross,OCP}$ should decrease as the temperature is lowered or the methanol solution is diluted [18,19]. As for $E_{cross,a}$, its value is dependent on the methanol crossover flux. With a given anodic limiting current, larger $i^*_{cross,OCP}$ will raise $E_{cross,a}$ and reduce the cell voltage. In contrast, $E_{cross,c}$ represents the intrinsic voltage loss at cathode due to methanol crossover. If θ is a characteristic value of the used catalyst, $E_{cross,c}$ could be regarded as a constant for a given MEA. For this reason, $E_{cross,c}$ should be independent of $i^*_{cross,OCP}$ and our fitting results (Tables 4 and 5) do demonstrate that $E_{cross,c}$ is nearly constant at 40 and 60 °C for the same MEA.

4.2. Cathodic and anodic polarization curve

Fig. 6 shows the polarizations of the cathode and anode individually based on our model. The anodic polarization curve was sensitive to temperature change, which implies that by raising temperature the improved power density of the whole cell is mainly due to the anodic side's improvement. By analyzing the anodic parameters, we believe the anodic polarization is dominated by the changes of $E_{0,a}$ and $E_{cross,a}$ responding to different temperatures. In addition, the cathodic polarization curve shown in Fig. 6 includes methanol crossover, in contrast to the cathodic polarization shown in Fig. 3, which does not include methanol crossover. This distinct difference between these two cathodic polarization curves represents the crossover effect significantly. Apparently, $E_{cross,c}$ and $i^*_{cross,OCP}$ are the key parameters of the cathodic performance curves. Besides, $i^*_{cross,OCP}$ which is sensitive to temperature is also tightly associated with $E_{cross,a}$. Again,

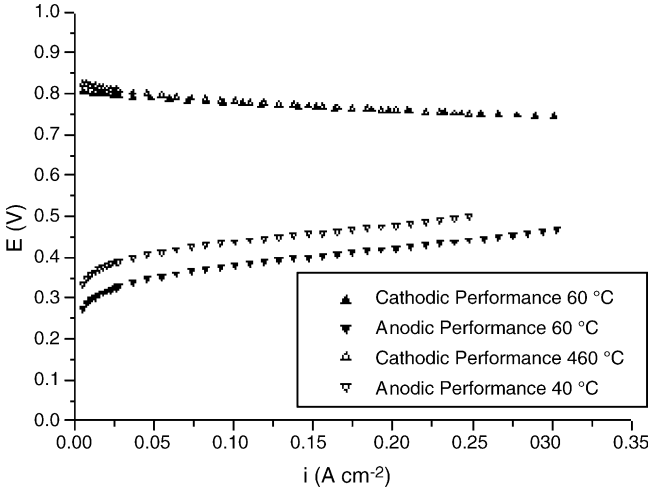

Fig. 6. The individual polarization behavior of anode and cathode at different temperatures (40 and 60 °C).

this proves that the anodic and cathodic crossover effects are interrelated.

4.3. Cell voltage loss due to individual overpotentials

Fig. 7 is a breakdown of overpotentials in our MEA experiments. It clearly illustrates the relative contribution of individual overpotentials. The activation overpotentials of both electrodes are the major cause of voltage loss, implying the importance of catalyst performance. The cathodic concentration overpotential is smaller than the concentration overpotential on the anode. This is due to excessive air flow on the cathode. The mass-transfer effect has a minor effect on the overpotential loss. In Fig. 7, the voltage loss due to the internal resistance becomes significant in the high-current region. In our model, the total voltage loss caused by methanol crossover can be defined as the difference between potential calculated from Eq. (14) and that calculated from Eq. (15) which eliminates the crossover effect ($\delta = 0$, $I_{\text{cross,OCP}} = 0$, $E_{\text{cross,a}} = 0$ $E_{\text{cross,c}} = 0$). Besides, the anodic and cathodic crossover effects can be further separated by comparing the anodic or cathodic part between Eqs. (14) and (15).

$$\begin{aligned} E_{\text{cell}} &= E_{\text{c}} - E_{\text{a}} - R_{\text{cell}} i^* \\ &= E_{0,\text{c}} - b_{\text{c}} \ln(i^*) + m_{\text{c}} \ln(1 - n_{\text{c}} i^*) - E_{0,\text{a}} \\ &\quad - b_{\text{a}} \ln(i^*) + m_{\text{a}} \ln(1 - n_{\text{a}} i^*) - R_{\text{cell}} i^* \end{aligned} \tag{15}$$

4.4. Impact of individual parameter on the cell performance

Activation overpotential, internal resistance, concentration overpotential of oxygen and methanol, and methanol crossover are the main causes for cell voltage loss. With proper MEA design and fabrication process, these overpotentials could be reduced. Figs. 8–12 illustrate how individual parameters can affect the cell performance (output voltage, E_{cell}, and power density, P). For simplicity, Eq. (15) was used and only changes in the cathodic parameters were introduced, and the anodic performance was calculated by fixing the anodic parameters at $E_{0,\text{a}} = 0.3$ V, $b_{\text{a}} = 0.02$ V e^{-1}, $m_{\text{a}} = 0.1$ V e^{-1} and $n_{\text{a}} = 2$ cm^2 A^{-1}.

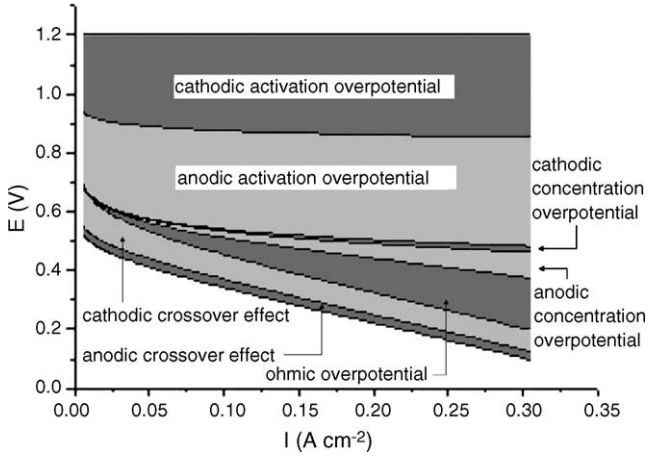

Fig. 7. The ratio of every overpotential in the entire current range at 60 °C.

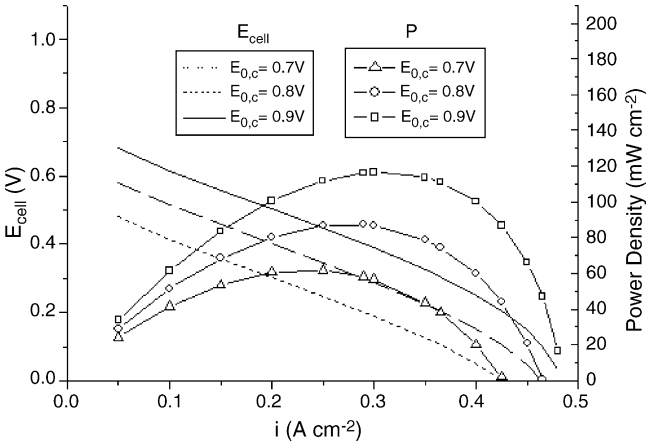

Fig. 8. The effects of $E_{0,\text{c}}$ ($b_{\text{c}} = 0.02$ V e^{-1}, $m_{\text{c}} = 0.05$ V e^{-1}, $n_{\text{c}} = 1$ cm^2 A^{-1} and $R_{\text{cell}} = 0.5\ \Omega$ cm^2).

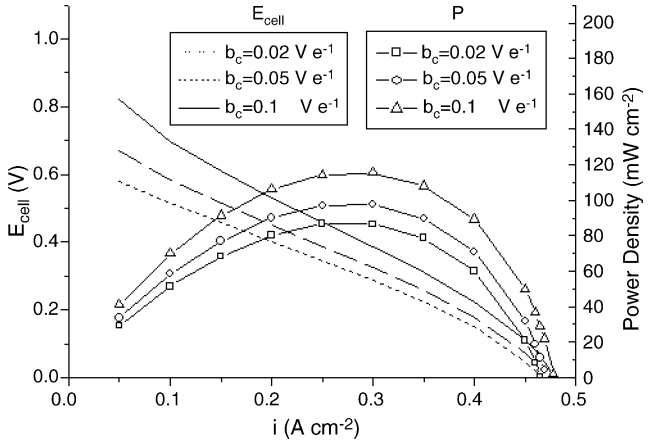

Fig. 9. The effects of b_{c} ($E_{0,\text{c}} = 0.8$ V, $m_{\text{c}} = 0.05$ V e^{-1}, $n_{\text{c}} = 1$ cm^2 A^{-1} and $R_{\text{cell}} = 0.5\ \Omega$ cm^2).

In fact, changes of anodic parameters would yield similar effects on cell performance. Both cell voltage (E) and power density (P) were plotted as functions of current density (i^*) on the same diagram.

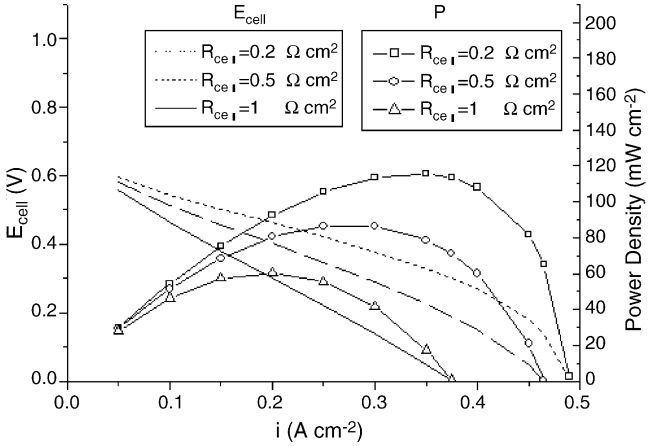

Fig. 10. The effects of R_{cell} ($E_{0,\text{c}} = 0.8$ V, $b_{\text{c}} = 0.02$ V e^{-1}, $m_{\text{c}} = 0.05$ V e^{-1} and $n_{\text{c}} = 1$ cm^2 A^{-1}).

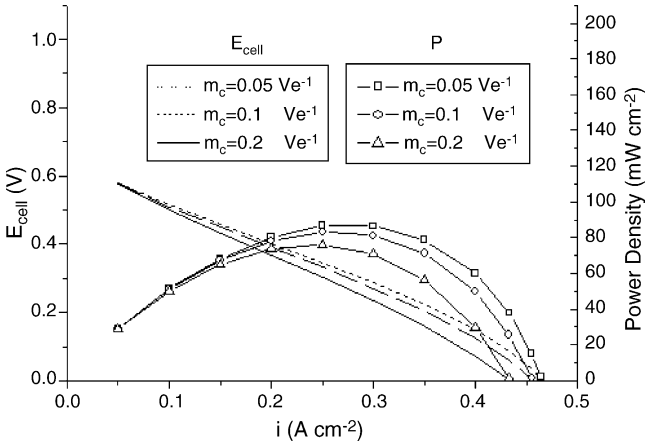

Fig. 11. The effects of m_c ($E_{0,c} = 0.8$ V, $b_c = 0.02$ V e^{-1}, $n_c = 1$ cm^2 A^{-1} and $R_{cell} = 0.5\ \Omega$ cm^2).

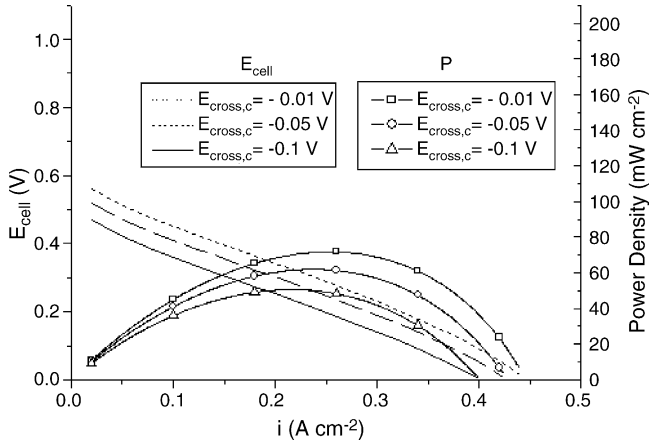

Fig. 13. The effects of $E_{cross,c}$ ($E_{0,c} = 0.8$ V, $b_c = 0.02$ V e^{-1}, $m_c = 0.05$ V e^{-1}, $R_{cell} = 0.5\ \Omega$ cm^2, $n_c = 1$ cm^2 A^{-1} and $i^*_{cross,OCP} = 0.05$ cm^2 A^{-1} (the calculated $E_{cross,a} = -0.044$ V)).

Besides operating condition, parameter $E_{0,c}$ and b_c were heavily related to the catalyst's inherent properties including its composition, structure and particle size. As shown in Fig. 8, variation of $E_{0,c}$ could greatly change the cell voltage at a given current density. The effect of b_c on the cell voltage (Fig. 9) would be more significant in the low current density region and less in the high current density region. By comparing Fig. 8 with Fig. 9, $E_{0,c}$ was more influential on the power density than b_c. So the increase of $E_{0,c}$ should be the main criterion for catalyst improvement.

Fig. 10 illustrates the effect of internal resistance on cell voltage and power density. Since the voltage loss due to the internal resistance is proportional to the current discharge, the voltage loss is significant in the high current density region. In Fig. 10, the current density where the cell delivered maximum power density was shifted to higher current densities as the internal resistant decreased.

The porosity, hydrophobicity and the thickness of the gas diffusion layer and catalyst layer all affect the transfer rate of the reacting species as well as the value of m_c and n_c as shown in Fig. 11 and Fig. 12. Water flooding on the cathode causes increases in m_c and n_c. Reducing m_c and n_c tend to increase the maximum power density and makes it shift to the high-current-density region. However, it seems the effects of m_c and n_c are minor because the anodic limiting current is small and dominates the overall mass-transfer overpotential.

$i^*_{cross,OCP}$, $E_{cross,a}$, and $E_{cross,c}$ are related to methanol crossover. Their influences on cell voltage and power density are shown in Figs. 13 and 14, respectively. In Fig. 13, $E_{cross,c}$ is similar to the additional activation overpotential at the cathode. As its definition, $E_{cross,c}$ is strongly associated with b_c and θ. Accordingly, a more methanol-tolerant catalyst may be helpful to improve the cell performance because a larger θ could reduce $E_{cross,c}$. Besides, the increase of b_c is also beneficial for the diminution of $E_{cross,c}$. On the other hand, $i^*_{cross,OCP}$ and $E_{cross,a}$ are reciprocal parameters. Fig. 14 shows the cell performances with different values of $i^*_{cross,OCP}$ and their corresponding $E_{cross,a}$ with unchanged limiting current density of the anode. Moreover, smaller m_a, which means better mass transfer at the anode, will be helpful to mitigate crossover effect.

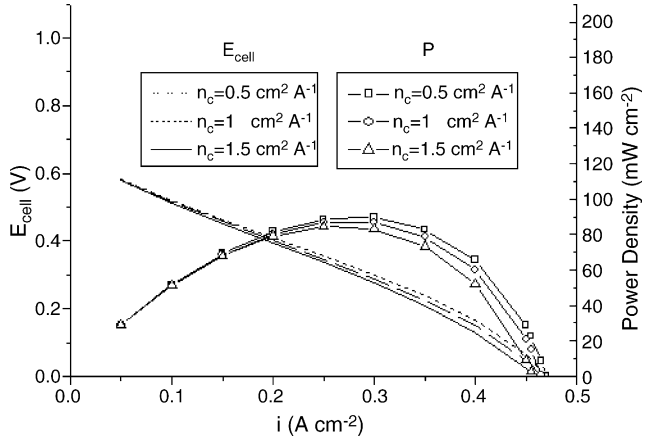

Fig. 12. The effects of n_c ($E_{0,c} = 0.8$ V, $b_c = 0.02$ V e^{-1}, $m_c = 0.05$ V e^{-1} and $R_{cell} = 0.5\ \Omega$ cm^2).

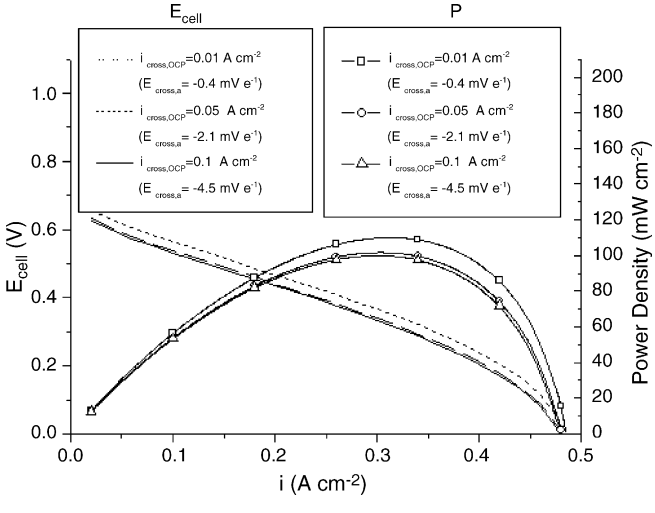

Fig. 14. The effects of $i^*_{cross,OCP}$ and $E_{cross,a}$ ($E_{0,c} = 0.8$ V, $b_c = 0.02$ V e^{-1}, $m_c = 0.05$ V e^{-1}, $R_{cell} = 0.5\ \Omega$ cm^2, $n_c = 1$ cm^2 A^{-1} and $E_{cross,c} = -0.05$ V).

5. Conclusion

A useful semi-empirical model was established for a DMFC in this work. This model can analyze anodic and cathodic voltage losses individually so that the controlling factors can be identified for a specific system. Parameters involved in this model include:

(i) Overpotentials of methanol oxidation reaction on the anode ($E_{0,a}$, and b_a).
(ii) Overpotential of oxygen reduction reaction on the cathode ($E_{0,c}$, and b_c).
(iii) Overpotential losses due to internal resistance (R_{cell}).
(iv) The effects of methanol crossover on the both anodic and cathodic potentials ($i^*_{cross,OCP}$, $E_{cross,a}$, and $E_{cross,c}$).
(v) Overpotentials due to the depletion of reacting species, such as oxygen (n_c and m_c) and methanol (n_a and m_a).

The impact and physical significance of major parameters can be summarized as follows:

(i) In the low current density region, the variations of $E_{0,c}$ and $E_{cross,c}$ are the major voltage losses at the cathode, and $E_{0,a}$ and $E_{cross,a}$ play the same role as $E_{0,c}$ and $E_{cross,c}$ at the anode.
(ii) In the intermediate current density region, ohmic and concentration overpotential are the key reasons causing the voltage drop.
(iii) With increases in the value of R, m and n, the maximum power density decreases and the current density accordingly drops.
(iv) $i^*_{cross,OCP}$ and $E_{cross,a}$ are inherently coupled. In other words, the anodic voltage is deeply influenced by the amount of methanol crossover flux.
(v) Improvement of both catalysts and mass transfer would be useful to reduce impact of the crossover effect, as characterized by $i^*_{cross,OCP}$, $E_{cross,c}$ and $E_{cross,a}$ in Eq. (14).

The performance of a single cell can be analyzed with this model to determine the factors that cause major voltage losses under various operating conditions, so that the performance of a DMFC can be optimized without too much trial-and-error.

Acknowledgements

Support from the National Science Council of Taiwan is appreciated. The authors also wish to thank Mr. F.-C Wu and Mrs. C.-P Huang for help in setting up experiment at initial stage, and the Material Research Laboratories of Industrial Technology Research Institute (ITRI), Taiwan, for financial assistance.

References

[1] M.L. Perry, T.F. Fuller, J. Electrochem. Soc. 149 (2002) S59–S67.
[2] L. Carrette, K.A. Friedrich, U. Stimming, CHEMPHYSCHEM 1 (2000) 162–193.
[3] L. Carrette, K.A. Friedrich, U. Stimming, Fuel Cells 1 (2001) 5–39.
[4] A.S. Arico, S. Srinivasan, V. Antonucci, Fuel Cells 1 (2001) 133–161.
[5] P. Costamagna, S. Srinivasan, J. Power Sources 102 (2001) 253–269.
[6] P. Costamagna, S. Srinivasan, J. Power Sources 102 (2001) 242–252.
[7] S. Srinivasan, E.A. Ticianelli, C.R. Derouin, A. Redondo, J. Power Sources 22 (1988) 359–375.
[8] J. Kim, S.M. Lee, S. Srinivasan, C.E. Chamberlin, J. Electrochem. Soc. 142 (1995) 2670–2674.
[9] G. Squadrito, G. Maggio, E. Passalacqua, F. Lufrano, A. Patti, J. Appl. Electrochem. 29 (1999) 1449–1455.
[10] D. Chu, R. Jiang, J. Power Sources 80 (1999) 226–234.
[11] K. Scott, P. Argyropoulos, K. Sundmacher, J. Electroanal. Chem. 477 (1999) 97–110.
[12] P. Argyropoulos, K. Scott, A.K. Shukla, C. Jackson, Fuel Cells 2 (2002) 78–82.
[13] P. Argyropoulos, K. Scott, A.K. Shukla, C. Jackson, J. Power Sources 123 (2003) 190–199.
[14] S. Wasmus, A. Küver, J. Electroanal. Chem. 461 (1999) 14–31.
[15] P.S. Kauranen, E. Skou, J. Munk, J. Electroanal. Chem. 404 (1996) 1–13.
[16] P.S. Kauranen, E. Skou, J. Electroanal. Chem. 408 (1996) 189–198.
[17] J. Munk, P.A. Christensen, A. Hamnett, E. Skou, J. Electroanal. Chem. 401 (1996) 215–222.
[18] Z.H. Wang, C.Y. Wang, J. Electrochem. Soc. 150 (2003) A508–A519.
[19] K.T. Jeng, C.W. Chen, J. Power Sources 112 (2002) 367–375.
[20] R. Jiang, D. Chu, J. Electrochem. Soc. 151 (2004) A69–A76.
[21] R. Jiang, D. Chu, Electrochem. Solid-State Lett. 5 (2002) A156–A159.
[22] J. Cruickshank, K. Scott, J. Power Sources 70 (1998) 40–47.
[23] S.F. Baxter, V.S. Battaglia, R.E. White, J. Electrochem. Soc. 146 (1999) 437–447.
[24] C. Marr, X. Li, J. Power Sources 77 (1999) 17–27.
[25] J.J. Baschuk, X. Li, J. Power Sources 86 (2000) 181–196.
[26] A.A. Kulikovsky, Fuel Cells 2 (2001) 162–169.